ISSN 2616-5805 Vol. 4, Issue 1: 32-43, DOI: 10.25236/AJMS.2023.040106

Bicycle Trajectory Control Based on Kinematic and Dynamical Models

Nuo Qiu[*], Yang Huang[#], Zixing Lu[#]

School of Mathematics, Science and Information Technology, Shaoxing University, Shaoxing, 312000, China
**Corresponding author: 349029008@qq.com*
[#]These authors contributed equally.

Abstract: *This paper uses a bicycle model as an example to explore its travel pattern and corresponding trajectory. The movement of the bicycle changes depends on the road conditions. The kinematic and dynamical models are used to explore its movement patterns in low and high speed states. A simplified version of the bicycle trajectory is obtained by controlling the deflection angle and the total body length. It is found that the front and rear wheel trajectories are concentric circles with the same point as the centre and different radii, and the position of the centre of mass affects the central trajectory. The model is applied to trajectory mapping to make a Taiji diagram.*

Keywords: *Unmanned Technology, Kinematic and Dynamical Models, Prediction Model, Track Mapping, Taiji diagram*

1. Introduction

Automated driving technology is a widely concerned issue today, with safe driving being a major concern for the public[1]. The trajectory of the wheels is an important focus in the study of safe vehicle driving. Considering the relative complexity of four-wheeled vehicles, this paper start with the trajectory of a two-wheeled bicycle and analyse the wheel trajectory at different speeds[2].

In 2008, Lychek Keo and Yamakita Masaki proposed a new trajectory tracking and balancing control algorithm that guarantees the stability of a bicycle even at zero linear velocity without the need for an auxiliary controller[3]. In 2011, they further optimised this with MATLAB XPC-TARGET on bicycle control, an autonomous electric bicycle can be remotely controlled from a single computer host[4]. In 2013, A. L. Schwab and J. P. Meijaard conducted a review study of bicycle dynamics and rider control, proposing open and promising directions for future work in the field of bicycle handling and control[5]. In 2014, Hongbin Ren et al. proposed a nonlinear bicycle model that includes the longitudinal, lateral and yaw motions of the vehicle. This bicycle model uses a simplified piecewise linear tyre model and a tyre force adjustment algorithm to produce closely matched vehicle trajectories over a wide range of vehicle operations compared to actual vehicles[6]. In 2019, Vineet Kosaraju et al. proposed Social-BiGAT, a graph-based generative adversarial network for generating realistic, multiple pedestrians in a scene multi-modal trajectory prediction for applications including control of autonomous vehicles and social robots, as well as security and surveillance[7]. In 2021, Leilei Cui et al. investigated the trajectory tracking problem for autonomous bicycles, achieving asymptotic trajectory tracking compared to most existing methods that only deal with approximate trajectory tracking[8]. In 2022, Kanghui He et al. proposed a learning-based control framework that framework is applicable to a class of underdriven bicycle robots that can achieve effective prediction by using event-triggered updates in the learning process, where tracking errors and roll angles are limited to a small range explicitly given[9].

The bicycle shown in Figure 1 assumes that the rear wheel is fixed and not steerable and that the front wheel is controlled by the handlebars and can be deflected by a certain angle. Figure 1(b) shows the projection of the wheel and beam on the table after the handlebars have been deflected by a certain angle. It is further assumed that the bicycle body remains perpendicular to the table during travel, that the front wheel deflection axis is perpendicular to the table and that there is no sliding friction between the wheel and the table during travel.

ISSN 2616-5805 Vol. 4, Issue 1: 32-43, DOI: 10.25236/AJMS.2023.040106

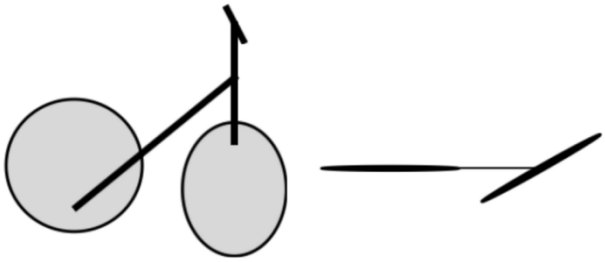

Figure 1: Schematic diagram of the bicycle stance

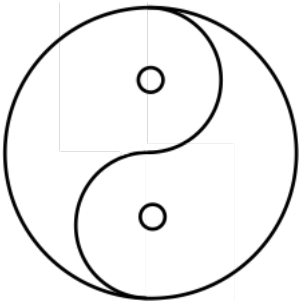

Figure 2: Simple Taiji diagram

In this paper we will develop mathematical models to investigate the travel patterns of a bicycle at high and low speeds, and use *MATLAB* mathematical software to draw mathematical models of the front and rear wheels.The tabletop is modelled as a real road, and urban road models and rural road models are developed for congested or open road scenarios, corresponding to low and high speed bicycle motion conditions.

Table 1: Description of symbols

Symbols	Description
L	Body length
θ	Body deflection angle
a	Acceleration
P	Bicycle centre of mass position
S_1	Distance from rear wheel to centre of mass
S_2	Distance from front wheel to centre of mass
θ_f	Front wheel steering angle
θ_r	Rear wheel steering angle
α	Slip angle
β	Yaw angle
V	Bicycle centre-of-mass speed
x_0	Bicycle horizontal coordinate position
y_0	Bicycle vertical coordinate position
F_f	Friction of the ground against the front wheels
F_r	Friction of the ground against the rear wheels
C_f	Front wheel linear steering stiffness
C_r	Front wheel linear steering stiffness

Figure 2 shows the traditional Chinese cultural symbol of Taiji, which will be mapped in this paper based on a dynamic structural model of the front and rear wheels to simulate bicycle autopilot technology.The Taiji diagram is divided into three parts.The outer circle, the fissure and the fisheye. As the fisheye and the outer circle are drawn in the same way, only the outer circle and the fisheye can be analysed.

ISSN 2616-5805 Vol. 4, Issue 1: 32-43, DOI: 10.25236/AJMS.2023.040106

The rest of this paper is organized as follows: Sections II and III respectively summarize the model construction and the trajectory control problems, underlying the specificity of each. Section IV explores the relationship between body length and deflection angle. Lastly, Section VI concludes this paper.

The symbols in this paper are described as follows table 1.

2. Model Construction

2.1 City Road Model

2.1.1 Kinematic modelling

The tabletop simulates a real-life, high-traffic roadway and is idealised as a kinematic model[10] without sliding friction. As the rear wheel is fixed and non-steerable, the direction of velocity of the current centre of mass can be approximated as the direction of velocity of the front wheel of the vehicle at low speeds.

Figure 3 shows that the bicycle can be considered as a control system. The control model is simplified as (a,θ) where a represents the acceleration of the bicycle, with positive acceleration inputted to the throttle and negative acceleration inputted to the brake. The bicycle travel pattern can be represented by the horizontal and vertical coordinates position and speed, i.e. the output (x,y,v) . The initial value of the control system[11] is set to (x_0,y_0,v) .

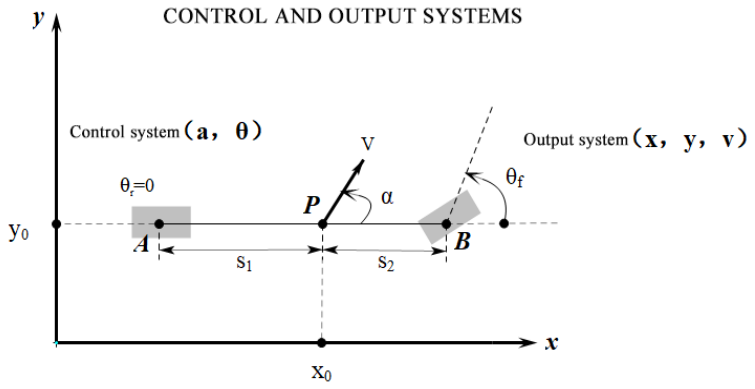

Figure 3: Control and output systems

2.1.2 Kinematic models for solutions

The effect of the bicycle on centripetal acceleration is minimal at low speeds.

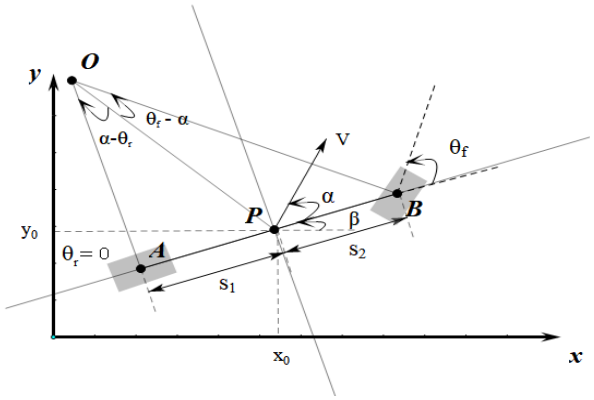

Figure 4: Bicycle kinematic model

The bicycle is considered as a mass P to be studied and analysed. The point O in Figure 4 represents the instantaneous centre of rotation of the vehicle and OP is the radius of its trajectory.

The kinematic laws of the bicycle are discussed by differentiating time into infinity for each small period of time and analysing the changes in each state quantity of the bicycle. The position and velocity

ISSN 2616-5805 Vol. 4, Issue 1: 32-43, DOI: 10.25236/AJMS.2023.040106

relationships at moments t and t+1 are established, with subscripts representing the moments corresponding to each physical quantity.

$$x_{t+1} = x_t + v_t \cos(\alpha + \beta) dt \tag{1}$$

$$y_{t+1} = y_t + v_t \sin(\alpha + \beta) dt \tag{2}$$

$$\beta_{t+1} = \beta_t + \frac{v_t \sin\alpha}{s_1} dt \tag{3}$$

$$v_{t+1} = v_t + adt \tag{4}$$

The relationship between the slip angle α[12] and the distance s from the center of mass and the handle rotation angle θ can be solved by plane geometry.

$$\alpha = \arctan \frac{s_1 \tan\theta_f + s_2 \tan\theta_r}{s_1 + s_2} \tag{5}$$

The rate of change of the bicycle yaw angle[13] is approximately equal to the angular velocity.

$$\psi_\beta = \frac{v \cos\alpha (\tan\theta_f - \tan\theta_r)}{s_1 + s_2} \tag{6}$$

At each moment the input to the system (x,y,v) is continuously varied by the control system (a,θ). As the rear wheel of the bicycle is fixed, $\theta_r = 0$. α and β change continuously as the control system θ_f changes, which in turn affects the position of the centre of mass of the bicycle.

Therefore, the travel pattern of the urban road model can be iteratively expressed as

$$\begin{cases} x_{t+1} = x_t + v_t \cos(\alpha + \beta) \ , \alpha = \arctan \dfrac{s_1 \tan\theta_f}{s_1 + s_2} \\ y_{t+1} = y_t + v_t \sin(\alpha + \beta) \ , \beta_{t+1} = \beta_t + \dfrac{v_t \sin\alpha}{s_1} dt \\ v_{t+1} = \lim\limits_{a \to 0} (v_t + adt) = v_t \ , \theta_r = 0 \end{cases} \tag{7}$$

The rate of change of the bicycle yaw angle (attitude information) at this point is

$$\psi_{\beta_{t+1}} = \psi_{\beta_t} + \frac{v_t \sin\alpha}{s_1} dt \tag{8}$$

2.2 Rural Road Model

2.2.1 Dynamics modelling

In the dynamics model[14], the centre of mass is acted upon by both centripetal and inertial accelerations[15], when position information and velocity are more difficult to represent, so we use the vehicle slip rate ψ_α and the yaw angular acceleration a_β to describe the bicycle travel pattern.

2.2.2 Dynamic models for solutions

When the bicycle speed is high, the velocity vectors of the front and rear wheels of the bicycle do not coincide with the direction of the wheels.

Newton's second law gives the force in the direction of the transverse axis.

$$F_f + F_r = ma \tag{9}$$

where F_f and F_r are the frictional forces of the ground on the front and rear wheels and there are two forces acting together in the acceleration a. Therefore there are two accelerations, the inertial acceleration a_1 at the centre of mass of the bicycle along the transverse axis and the centripetal acceleration a_2 due to

ISSN 2616-5805 Vol. 4, Issue 1: 32-43, DOI: 10.25236/AJMS.2023.040106

the change in body orientation around the centre of rotation *O*.

We set the rate of change of slip angle and yaw angle be ψ_α, ψ_β. The transverse velocity is *vsinα* and the longitudinal velocity is *vcosα by d*ecomposing the velocity vector. Therefore, the transverse and centripetal accelerations at high speed are

$$a_1 = v\cos(\alpha\psi_\alpha)\psi_\alpha = v\psi_\alpha \tag{10}$$

$$a_2 = v\psi_\beta \tag{11}$$

$$a = a_1 + a_2 = v(\psi_\alpha + \psi_\beta) \tag{12}$$

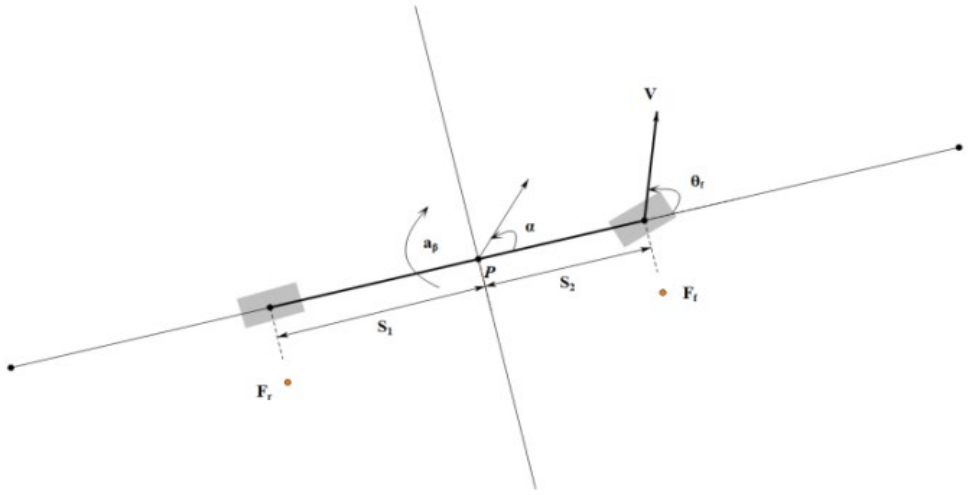

Figure 5: Torque balance model

Figure 5 represents the torque balance equation[16]

$$I\psi_\beta = s_1F_r - s_2F_f \tag{13}$$

where *I* is the inertia of the bike[17] and F_f, F_r are the frictional forces of the ground on the front and rear wheels.

According to the principle of physics tyre lateral force and small slip angle there is a proportional relationship, the slip angle is the angle between the direction of the tyre[18] and the wheel speed vector. We set *Cf*, *Cr* for the front and rear wheel linear steering stiffness[19], αf、α_r front and rear wheel slip angle, according to the proportionality coefficient can be derived from the size of the sassafras force.

$$F_f = C_f\alpha_f = C_f\left(\theta_f - \alpha - \frac{s_2\psi_\beta}{v}\right) \tag{14}$$

$$F_r = C_r\alpha_r = C_r\left(-\alpha + \frac{s_1\psi_\beta}{v}\right) \tag{15}$$

Substituting the frictional forces into the equation Newton's second law and the torque balance equation gives the vehicle slip rate ψ_α and the yaw angle acceleration a_β.

$$\psi_\alpha = \frac{-(C_f + C_r)\alpha}{mv} + \left(\frac{C_rs_1 - C_fs_2}{mv^2} - 1\right)\psi_\beta + \frac{C_f\theta_f}{mv} \tag{16}$$

$$a_\beta = \frac{C_rs_1 - C_fs_2}{I}\alpha + \frac{C_rs_1^2 + C_fs_2^2}{Iv}\psi_\beta + \frac{C_fs_2}{I}\theta_f \tag{17}$$

2.3 Wheel track plotting

We tend to consider the general body of the model directly to obtain a general solution. Determine

ISSN 2616-5805 Vol. 4, Issue 1: 32-43, DOI: 10.25236/AJMS.2023.040106

the deflection angle θ and the axis distance L (distance between the centre of the front and rear wheels), and draw concentric circle trajectories for the front and rear wheels with the same point as the centre and different radii.On a microscopic level, the points on any trajectory are perpendicular to the direction of travel of the wheels, as the question assumes that the body is always perpendicular to the table. It is only at the same point in time that the relative positions of the front and rear wheels will also be constrained by θ and L, resulting in different trajectories. Therefore, different θ and L will cause the radii of the trajectories of the front and rear wheels to differ. Our simplified motion diagram is shown in Figure 6.

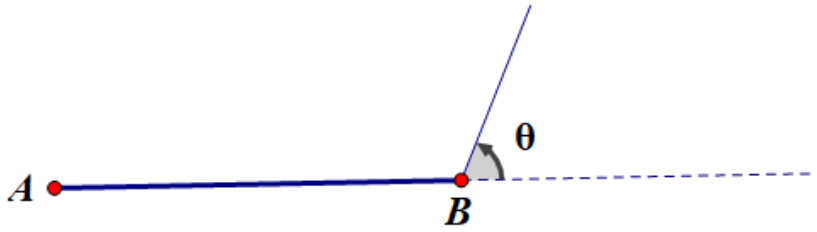

Figure 6: Simplification of the motion picture

2.3.1 Dynamic structure operation

Point A is the tangent point between the rear wheel and the rear wheel trajectory, point B is the tangent point between the front wheel and the front wheel trajectory, and line AB is the body length L. The frame is fixed after θ and L have been set.

Figure 7 shows the dynamic structure. When this frame is fixed and starts to move, the concentric circle centres, the size circle radii are fixed by the constraints of θ and L. The diagram below shows the analysis process.

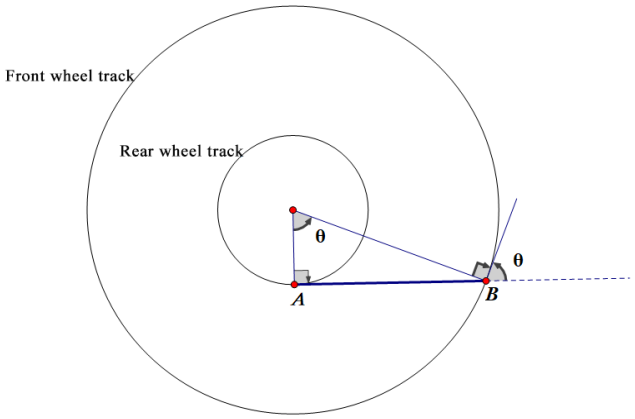

Figure 7: Dynamic structural model

It is obvious that both points A and B are tangent points and that the radii of the front and rear wheel trajectories are $L/sin\theta$, $L/tan\theta$.

The angle between the tangent point of the front and rear wheels and the line connecting the centre of the circle at a fixed moment is the angle of deflection θ. The operating mode of this dynamic structure is the model diagram above.

2.3.2 Change in position of the centre of mass

Figure 8 shows that the centre of mass is at the centre of AB.

ISSN 2616-5805 Vol. 4, Issue 1: 32-43, DOI: 10.25236/AJMS.2023.040106

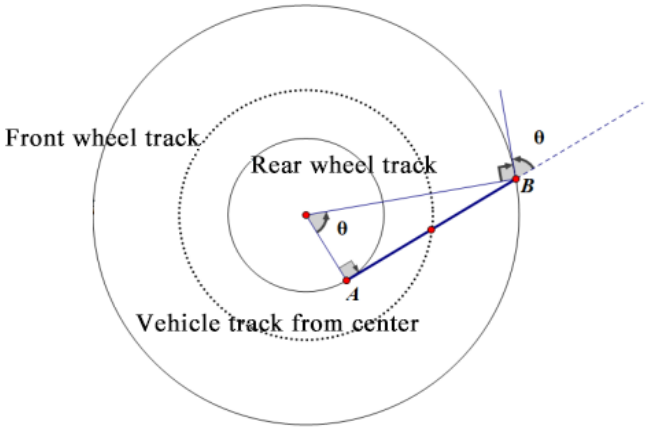

Figure 8: Uniform mass distribution

Figure 9 shows that the centre of mass is not at the centre of AB.

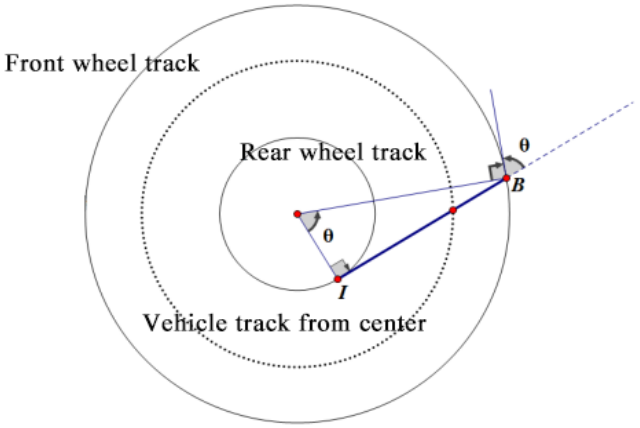

Figure 9: Uneven mass distribution

As the diagram shows, changing the centre of mass only affects the central trajectory and does not result in a change in the inner or outer trajectory.

2.3.3 Model implementation

In the dynamic structural model, the frame has a fixed concentric circle centre and small and large circle radii subject to the deflection angle θ and axis distance L constraints. The centre of gravity only affects the central trajectory and does not lead to a change in the inner and outer trajectories. The front and rear wheel trajectories are concentric circles with the same point as the centre and different radii for the front and rear wheels.

3. Track mapping

3.1 Drawing the outer circle

The problem of drawing a positive circle with a fixed bicycle steering angle θ and a given body length L is solved by looking at the external circle. The brush is located at the centre of mass to draw the circle with the deflection angle θ and the body length L set.

The trajectory left by removing the front and rear wheels is the graph drawn for the position of the centre of mass. The centre of mass can be found by assuming that the centre of the circle is the origin of the two-dimensional axis. The radius of the circle is then drawn and used as the outer circle of the Taiji diagram.

Next, we calculate the radius of the circle. Figure 10 below shows the outer circle of the Taiji with $\theta = \theta_1$ and $L = L_1$.

ISSN 2616-5805 Vol. 4, Issue 1: 32-43, DOI: 10.25236/AJMS.2023.040106

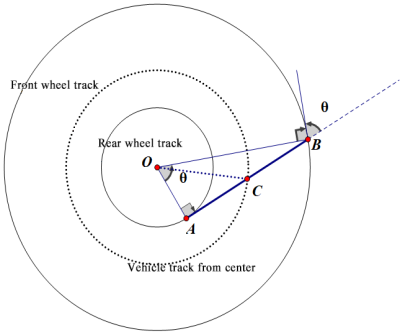

Figure 10: Taiji outer diagram

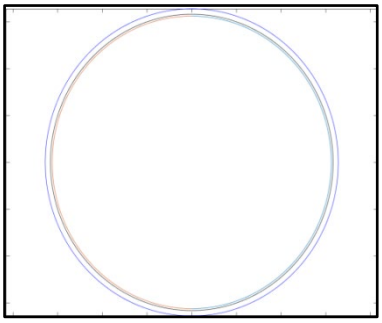

Figure 11: Centre of mass and front and rear wheel centre trajectories

The trajectory of the inner and outer wheels corresponding to this circle in Figure 11 is the circle drawn with radii *OA* and *OB*. *OC* is the radius of the circle of the Taiji diagram.

$$OC = \sqrt{\left(\frac{L}{\tan\theta}\right)^2 + \left(\frac{L}{2}\right)^2} \tag{18}$$

3.2 Drawing the fish line

The inner fish line is drawn by taking half of each of the two circles with the outer radius as the diameter, we determine the centres of the two circles as (0, *OC*/2) and (0, -*OC*/2) and the radius as *OC*/2. Half of each side is drawn in Figure 12.

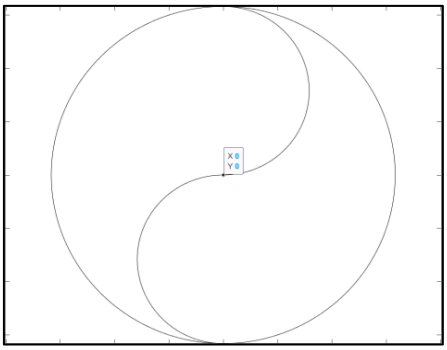

Figure 12: Internal fishing line

Next we discuss how to determine the trajectory of the two inner and outer reels when drawing the line. We set the axis length to $L = L_1$ and disregard the previous theta factor. The analysis proceeds as follows.

As the trajectory is drawn from (0, *OC*), the topmost bottom, the centre of gravity should be at (0, *OC*) when you first start drawing. With the front wheel inside the circle and the outer wheel outside the circle, the final trajectory is the blue dashed line as shown in Figure 13.

ISSN 2616-5805 Vol. 4, Issue 1: 32-43, DOI: 10.25236/AJMS.2023.040106

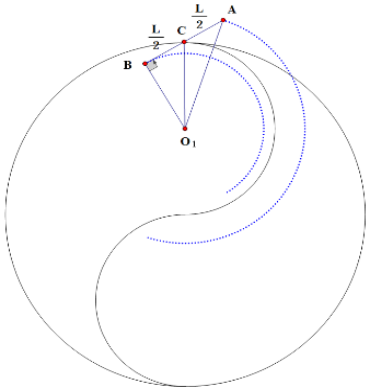

Figure 13: Final trajectory diagram

We zoom in on it partially for analysis in Figure 14.

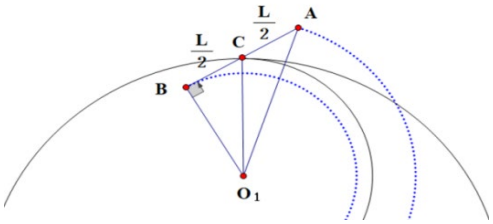

Figure 14: Local enlargement

Define O_1 = (0, OC/2) as the midpoint of the fish line at that time, with point C as the starting point and the centre of gravity of the bike.

$$O_1C = \frac{OC}{2} = \frac{\sqrt{\left(\frac{L}{\tan\theta}\right)^2 + \left(\frac{L}{2}\right)^2}}{2} \tag{19}$$

Combining the definition O_1B with the perpendicular to AB, we can find the radius of the inner trajectory circle $O_1B = \sqrt{O_1C^2 - BC^2}$, the radius of the outer trajectory circle $O_1A = \sqrt{O_1B^2 - AB^2}$.

Selecting the positions of the front and rear wheel starting points A and B, we let the point B be (x, y). Points A and B are symmetrical about point C. The endpoints are the points A and B symmetrical according to O_1, and then the half-circle is obtained by drawing the circle with the radius, and the lower half is obtained in the same way.

3.3 Error analysis

In the case of fixed L,θ has also been determined at a certain point. However, some unknown error leads to a slight deviation in θ, when the position condition is shown in the following equation[20].

$$\begin{cases} x_{t+1} = x_t + v_t\cos(\alpha+\beta)\ , \alpha = \arctan\dfrac{s_1\tan\theta_f}{s_1+s_2} \\ y_{t+1} = y_t + v_t\sin(\alpha+\beta)\ , \beta_{t+1} = \beta_t + \dfrac{v_t\sin\alpha}{s_1}dt \\ v_{t+1} = \lim\limits_{a\to 0}(v_t + adt) = v_t\ , \theta_r = 0 \end{cases} \tag{20}$$

As known from the equation, x_{t+1} ′ and y_{t+1} ′ produce a change in the distance of the change, which is the amount of the resulting fine error. We divide the amount of minor deviation in distance by the amount of change in θ to portray the magnitude of the error produced by the following equation.

ISSN 2616-5805 Vol. 4, Issue 1: 32-43, DOI: 10.25236/AJMS.2023.040106

$$\begin{cases} x'_{t+1} = x_t + v_t \cos(\alpha_1 + \beta), \alpha = \arctan \dfrac{s_1 \tan(\theta_f + \Delta\theta)}{s_1 + s_2} \\ y'_{t+1} = y_t + v_t \sin(\alpha_1 + \beta) \end{cases} \tag{21}$$

We use the relationship between the deviation distance and the dependent variable θ to represent the error δ.

$$\delta = \frac{\sqrt{(x_{t+1} - x'_{t+1})^2 + (y_{t+1} - y'_{t+1})^2}}{\Delta\theta} \tag{22}$$

When specific values are available, the magnitude of the length error with respect to the theta error can be calculated by substituting the formula.

4. Modeling Extension

Depending on how it is plotted, it can be extended to the plotting of any known curve. We simply need to know the expression of the curve and derive the equation of the tangent line at each point to design the plotted path. In the following we take discrete values to explore the relationship between L and θ.

(1) First we fix the angle of deflection θ. The axis lengths L are taken to be 1m, 2m and 3m respectively to plot the image , as shown in Figure 15 and Figure 16.

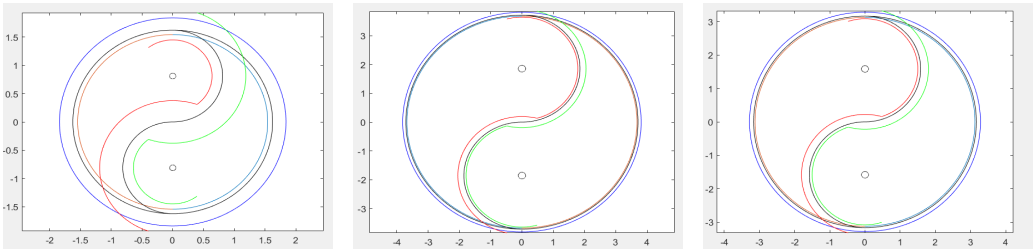

L = 1m θ = 50 rad *L = 2m θ = 50 rad* *L = 3m θ = 60 rad*

Figure 15: The image when L are taken to be 1m, 2m and 3m

Then we consolidate them into a single diagram.

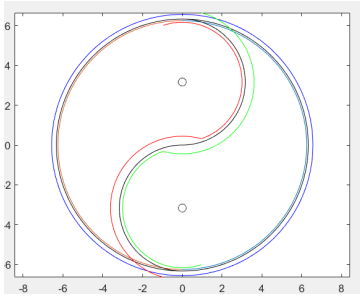

L = 1,2,3 m θ = 50 rad

Figure 16: The combined diagram when L = 1,2,3 m θ = 50 rad

It is clear that when the deflection angle θ is fixed, the front and rear wheels and the centre of mass trajectory are scaled up equally with L.

(2) Then fix the axis length L. θ is taken as 10 rad, 50 rad and 60 rad to plot the image , as shown in Figure 17 and Figure 18.

ISSN 2616-5805 Vol. 4, Issue 1: 32-43, DOI: 10.25236/AJMS.2023.040106

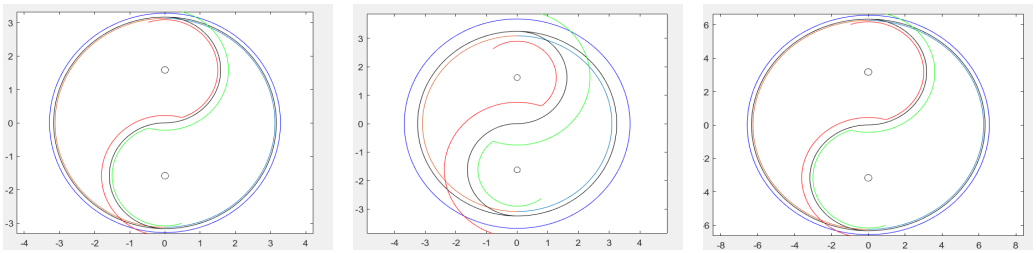

L = 2m θ = 10 rad L = 2m θ = 50 rad L = 2m θ = 60 rad

Figure 17: The image when θ is taken as 10 rad, 50 rad and 60

Subsequently, we consolidate them into a single diagram.

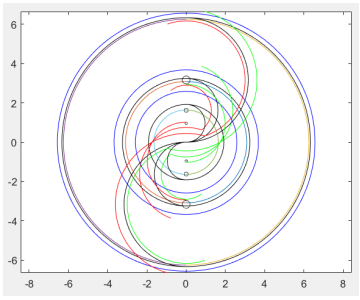

L = 2m θ = 10,50,60 rad

Figure 18: The combined diagram when L = 2m θ = 10,50,60 rad

It is clear that when fixing the axis length L, the flexibility of θ is relatively large and there is no obvious linear relationship[21].

5. Conclusions

Bicycle motion is different at low and high speeds and needs to be analysed by combining different physical quantities in kinematic and dynamical models. In the dynamic structure model, different deflection angles and axis distances affect the trajectory of the front and rear wheels. The position of the centre of mass only affects the central trajectory and does not lead to a change in the inner and outer trajectory. The front and rear wheel trajectories are concentric circles of the front and rear wheels with the same point as the centre and different radii. Various trajectories can be plotted according to the laws of bicycle motion. The authors will build a more comprehensive physics model to analyse the bicycle's operation and further find the limiting relationship between L and θ to make the model more comprehensive in the future.

Acknowledgements

The authors gratefully acknowledge the financial support from Shaoxing Academy of Arts and Sciences Scientific Research Projects.

References

[1] Xiong J, Li B, Yu R, et al. Reduced dynamics and control for an autonomous bicycle[C]. 2021 IEEE International Conference on Robotics and Automation (ICRA).
[2] Ziegler C, Willert V, Adamy J. Modeling Driving Behavior of Human Drivers for Trajectory Planning [J]. IEEE Transactions on Intelligent Transportation Systems, 2022, 23(11): 20889-20898.
[3] Lychek Keo and Yamakita Masaki, "Trajectory control for an autonomous bicycle with balancer," 2008 IEEE/ASME International Conference on Advanced Intelligent Mechatronics, Xi'an, China, 2008, pp. 676-681.
[4] Keo L, Yamakita M. Control of an autonomous electric bicycle with both steering and balancer controls [J]. Advanced Robotics, 2011, 25(1-2): 1-22.
[5] Schwab A L, Meijaard J P. A review on bicycle dynamics and rider control [J]. Vehicle system dynamics, 2013, 51(7): 1059-1090.

ISSN 2616-5805 Vol. 4, Issue 1: 32-43, DOI: 10.25236/AJMS.2023.040106

[6] Ren H, Shim T, Ryu J, et al. Development of effective bicycle model for wide ranges of vehicle operations[R]. SAE Technical Paper, 2014.
[7] Kosaraju V, Sadeghian A, Martín-Martín R, et al. Social-bigat: Multimodal trajectory forecasting using bicycle-gan and graph attention networks [J]. Advances in Neural Information Processing Systems, 2019, 32.
[8] Bellegarda G, Quan N. Dynamic Vehicle Drifting With Nonlinear MPC and a Fused Kinematic-Dynamic Bicycle Model[J]. IEEE Control Systems Letters, 2022(6-).
[9] He K, Deng Y, Wang G, et al. Learning-based trajectory tracking and balance control for bicycle robots with a pendulum: A Gaussian process approach [J]. IEEE/ASME Transactions on Mechatronics, 2022, 27(2): 634-644.
[10] Ekaso D, Nex F, Kerle N. Accuracy assessment of real-time kinematics (RTK) measurements on unmanned aerial vehicles (UAV) for direct geo-referencing [J]. Geo-spatial information science, 2020, 23(2): 165-181.
[11] Park J, Sandhu R. Towards usage control models: beyond traditional access control[C]. Proceedings of the seventh ACM symposium on Access control models and technologies. 2002: 57-64.
[12] Hac A, Simpson M D. Estimation of vehicle side slip angle and yaw rate [J]. SAE transactions, 2000: 1032-1038.
[13] Rone W, Ben-Tzvi P. Dynamic modeling and simulation of a yaw-angle quadruped maneuvering with a planar robotic tail [J]. Journal of Dynamic Systems, Measurement, and Control, 2016, 138(8).
[14] Mettler B, Tischler M B, Kanade T. System identification of small-size unmanned helicopter dynamics[C]. Annual Forum Proceedings- American Helicopter Society. 1999, 2: 1706-1717.
[15] Leff H S. Acceleration for circular motion [J]. American Journal of Physics, 2002, 70(5): 490-492.
[16] Ushakumari S, Nair P S C, Sankaran R. Closed Loop Performance of A Permanent Magnet Brushless dc Motor Incorporating the Nonlinearity in Torque-Balance Equation (Transient Operation)[J]. Electric Power Components and Systems, 2002, 30(12): 1249-1260.
[17] Zhang Y, Chen K, Yi J. Rider trunk and bicycle pose estimation with fusion of force/inertial sensors [J]. IEEE Transactions on Biomedical engineering, 2013, 60(9): 2541-2551.
[18] Matas J P, Morris J F, Guazzelli E. Lateral forces on a sphere[J]. Oil & gas science and technology, 2004, 59(1): 59-70.
[19] Rouhi M, Ghayoor H, Hoa S V, et al. Effect of structural parameters on design of variable-stiffness composite cylinders made by fiber steering [J]. Composite Structures, 2014, 118: 472-481.
[20] Schachter J. An error in error analysis 1[J]. Language learning, 1974, 24(2): 205-214.
[21] Ellis A B. Connections between generalizing and justifying: Students' reasoning with linear relationships [J]. Journal for Research in Mathematics education, 2007, 38(3): 194-229.